Chiang Mai J. Sci. 2019; 46(5) : 1001-1008
http://epg.science.cmu.ac.th/ejournal/
Contributed Paper

Role of Sb-dopant on Physical and Optical Properties of ZnO Thin Film Deposited by Sol-gel-based Coating Method

Wuttichai Sinornate [a], Hidenori Mimura [b] and Wisanu Pecharapa*[a]

[a] College of Nanotechnology, King Mongkut's Institute of Technology Ladkrabang, Bangkok 10520, Thailand.

[b] Research Institute of Electronics, Shizuoka University, 3-5-1 Johoku, Naka-ku, Hamamatsu-shi, Shizuoka, 432-8011, Japan.

*Author for correspondence; e-mail: kpewisan@gmail.com

Received: 22 February 2019
Revised: 19 June 2019
Accepted: 21 June 2019

Abstract

Sb-doped ZnO films were prepared by sol-gel spin coating technique on glass substrate. The sol-gel was prepared from zinc acetate dihydrate as zinc precursor and diethanolamine as sol stabilizer. Antimony (III) acetate was selected as the precursor of Sb. The doping concentration was varied from 0 to 10 mol%. The films were prepared by spin coating technique following by annealing at 500°C for 2 h in ambient air. The XRD exhibits ZnO hexagonal wurtzite without impurity phase. Their XRD peaks show deterioration in crystallinity that is in accordance with FESEM and TEM images showing decreasing in particle size with increasing doping content. The XPS confirm the existence of Sb^{3+} that could substitute Zn^{2+} on the zinc site or zinc vacancy. The photoluminescence results exhibit blue-shift with increasing Sb doping concentration. The transmittance spectra show high transmittance above 90% in visible region.

Keywords: thin film, Sb-doped ZnO, sol-gel method

1. Introduction

ZnO is recognized as an intrinsic n-type semiconductor with such wide energy band gap of 3.37 eV and a large exciton binding energy of 60 meV at room temperature. Zinc oxide (ZnO) has been extensively applied for many fields of applications such as transparent conductive electrode, piezoelectric device, UV sensor and gas sensor [1-4]. High quality p-n junction structure is acknowledged as one of effective approaches to fabricate high performance semiconductor devices. Furthermore, p-type ZnO is still in challenge and may be achieved by substitution of group-VA element (P, Sb) on O-site [5, 6] and transition metal (Cu, Ag) on Zn-site [7, 8]. Antimony is considered as a good candidate for producing a shallow acceptor state in ZnO if they can substitute at the O sites and Zn sites [6, 9].

Many different processes have been extensively employed for preparing well-defined p-type ZnO. Kim *et al.* [9] deposited Ag-doped ZnO by hot-walled pulsed laser deposition (HW-

PLD) and reported that the doped films were p-type with blue shift in photoluminescence. Dang *et al.* [10] reported the deposition of p-type ZnO thin films by doping with mixed antimony and tin via DC magnetron sputtering. Cheng *et al.* [11] prepared p-type Sb-doped ZnO thin films by metal organic chemical vapor deposition method (MOCVD). Noh *et al.* [12] gave a report on the preparation of ZnO thin films dually doped with Ga, P by pulsed laser deposition (PLD) and the deposited films exhibited p-type electrical conductivity. Among these techniques, sol-gel spin coating technique has been widely used for depositing various metal-oxide based thin films because of considerable advantages comparing to the others such as low-cost precursor, low-cost system, simple deposition equipment.

In this work, we report the fabrication and characterization of Sb-doped ZnO thin films prepared by sol-gel spin coating technique on glass substrate with various doping concentrations and mild annealing. The effect of doping concentration on physical and optical properties of ZnO thin films were extensively investigated.

2. MATERIALS AND METHODS

Sb-doped ZnO films were prepared by sol-gel spin coating technique on glass substrate. First, zinc acetate dihydrate designated as zinc precursor was dissolved in absolute ethanol and 1 ml of diethanolamine was used as a sol stabilizer. The mixture was stirred with magnetic stirrer until the sol-gel was clear followed by the addition of doping precursor. Antimony (III) acetate was selected as the precursor of Sb. The doping concentration was varied from 0 to 10 mol%. The mixture of zinc and dopant precursor was stirred followed by heating at 75°C for 2 h before aging for 24 h. The glass substrates were cleaned by sonication in deionized water, acetone, methanol and isopropanol for 10 min, respectively. The bare ZnO and doped ZnO thin films were spun at 2000 rpm for 30s. For each coating, the coat film was soft baked at 100°C for removing solvent, proceeding hydrolysis and thermal decomposition of acetate precursor and the coating was proceeded and repeated 8 times. After the spinning process the deposited films were annealed at 500°C for 2 h in air.

The structural properties of the prepared films were investigated by Rigaku SmartLab X-ray diffractometer (XRD) with CuK_{α} radiation (λ = 1.54178 Å). The surface morphology and thickness of the films were monitored by Hitachi S4700 field emission scanning electron microscope (FESEM). Transmission electron microscope (TEM) images of the prepared films were monitored using a JEOL JEM-ARM200F. The existence and oxidation state of Sb dopant were carried out by X-ray photoelectron spectroscopy measurement (XPS) PHI5000 VeralProbll@Ulvac-PHI, Inc, JAPAN using AlK_{α} at the beamline 5.3 of the Synchrotron Light Research Institute (SLRI), Nakhon Ratchasima, Thailand. Photoluminescence (PL) was recorded at room temperature by using Edinburgh Instruments FLS980 ($\lambda_{excitation}$ = 325 nm). The optical transmittance was examined by a UV-vis spectroscopy (Thermo Scientific Orion AquaMate 8000) in the wavelength range of 325-800 nm.

3. RESULTS AND DISCUSSION

Figure 1 shows X-ray diffraction patterns of ZnO thin films with various doping concentrations. The diffraction patterns are nicely matched with hexagonal wurtzite zinc oxide phase (ICSD no. 157724) without any impurity phases. Moreover, the diffracted peak position of the doped films remains at the same position, implying the good incorporation of the Sb dopant in ZnO matrix. The result additionally indicates significant decrease in peak intensity, reflecting the deterioration in crystallinity of ZnO with increasing Sb doping concentration. Due to the slight difference

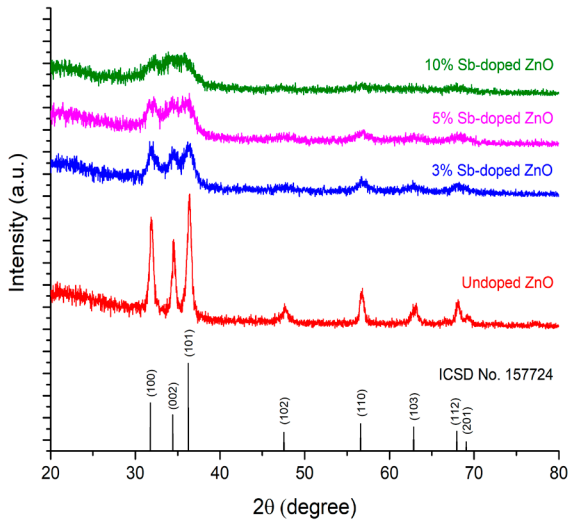

Figure 1. XRD pattern of Sb-doped ZnO thin films with various doping concentrations.

in ionic radius of Sb^{3+} (r=0.76 Å) [13] and Zn^{2+}(r=0.72 Å) [14], incorporated Sb^{3+} could substitute Zn^{2+} site in ZnO lattice, resulting in generation of local stress in the lattice and prevention of crystal growth of ZnO.

The morphologies of undoped and Sb-doped ZnO thin films with different doping concentrations are illustrated in Figure 2 (a)-(d). These results exhibit the composition of ZnO nanoparticles. As observed in SEM images, the size of ZnO nanoparticles significantly decreases with increasing Sb doping content that is well agreeable with the broadening of major XRD peaks clearly observed in Figure 1. The inset of Figure 4 exhibits cross section of undoped and Sb-doped ZnO films. The results show the uniform thickness of the prepared films with average thickness of 75 to 115 nm. The thickness of undoped film is greater than the doped films due to the composition of nanoparticles with greater particle size of the undoped film that can result in the porous film with greater thickness. The porosity of the ZnO films prepared by sol-gel spin coating technique is the result from the decomposition of acetate group of zinc acetate precursor during annealing process.

Transmission electron microscope were employed to characterize these structures in detail. TEM images of undoped and Sb-doped ZnO thin films with various doping concentrations are illustrated in Figure 3 (a)-(d). In addition, energy-dispersive X-ray spectroscopy was conducted to confirm the existence and chemical composition of relevant elements in the prepared samples. The corresponding EDS mapping and spectra are illustrated in the insets of each TEM image. The results exhibit that the undoped ZnO consists of only Zn and O. Meanwhile, the doped samples exhibit the existence of Sb element with increasing content when the film was doped with higher content of Sb dopant. The corresponding TEM images clearly reveal the considerable decrease of particle size when the film is incorporated with Sb. The chemical composition from EDS analysis and the average size diameter of all samples are presented in Table 1.

In order to identify the presence of Sb in the ZnO, bonding and oxidation state, it is

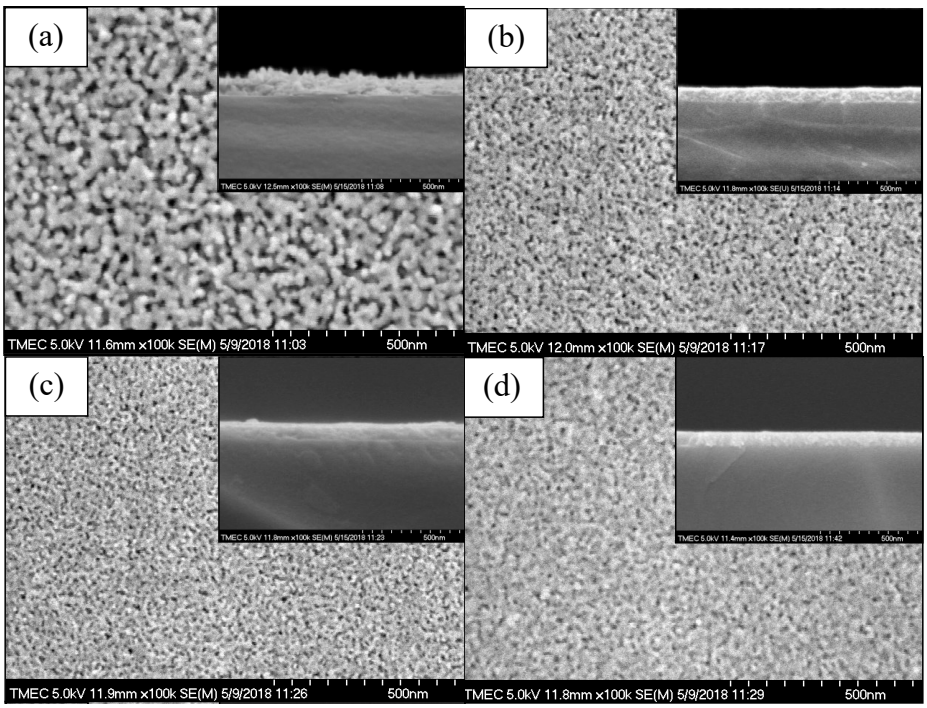

Figure 2. Surface morphologies and cross section images (inset) of (a) Undoped ZnO, (b) 3% Sb-doped ZnO, (c) 5% Sb-doped ZnO, (d) 10% Sb- doped ZnO.

necessary to perform the X-ray photoelectron spectroscopy (XPS) analysis. Figure 4 (a) displays the survey XPS spectra of 5% Sb-doped ZnO thin films. In this analysis, the C1s peak at 284.8 eV was used for calibration. The results show the presence of Zn, O, and Sb element in the doped films. It is observed that the characteristic peaks of antimony Sb $3d_{3/2}$ and Sb $3d_{5/2}$ are located at 539.1 eV and 529.8 eV, respectively, indicating the incorporation Sb dopant in ZnO thin film. Furthermore, the deconvolution of Sb $3d_{3/2}$ suggests that the oxidation state of antimony is Sb^{3+} that is in accordance with the starting antimony precursor. On the other hand, the difference of spin-orbit splitting of 23.1 eV for Zn $2p_{1/2}$ (1044.2 eV) and Zn $2p_{3/2}$ (1021.1 eV) confirms that the Zn atom are completely ZnO with Zn^{2+} bound with oxygen [15]. As the proposed by Senthil et al [16] the substitution of Sb^{3+} on Zn^{2+} can change the conductivity from n-type to p-type.

PL measurement was performed to prove the formation of acceptor level in these samples. Figure 5 shows PL spectra of undoped and Sb-doped ZnO thin films excited by xenon arc lamp (l=325 nm). All samples exhibit UV emission peak at 384 nm with a weak visible emission at 700 nm corresponding to near band edge emission (NBE) and deep-level emission, respectively. As observed in Figure 5, the NBE of Sb-doped ZnO thin films presents a slight blue shift (inset of Figure 5). This shift behavior of NBE is could be related to the substitution of Sb^{3+} at Zn^{2+} site or zinc vacancy site in ZnO lattice [15, 16]. The increase of optical band gap with increasing Sb doping concentration may be attributed to the increase the carrier concentration of the doped film regarding

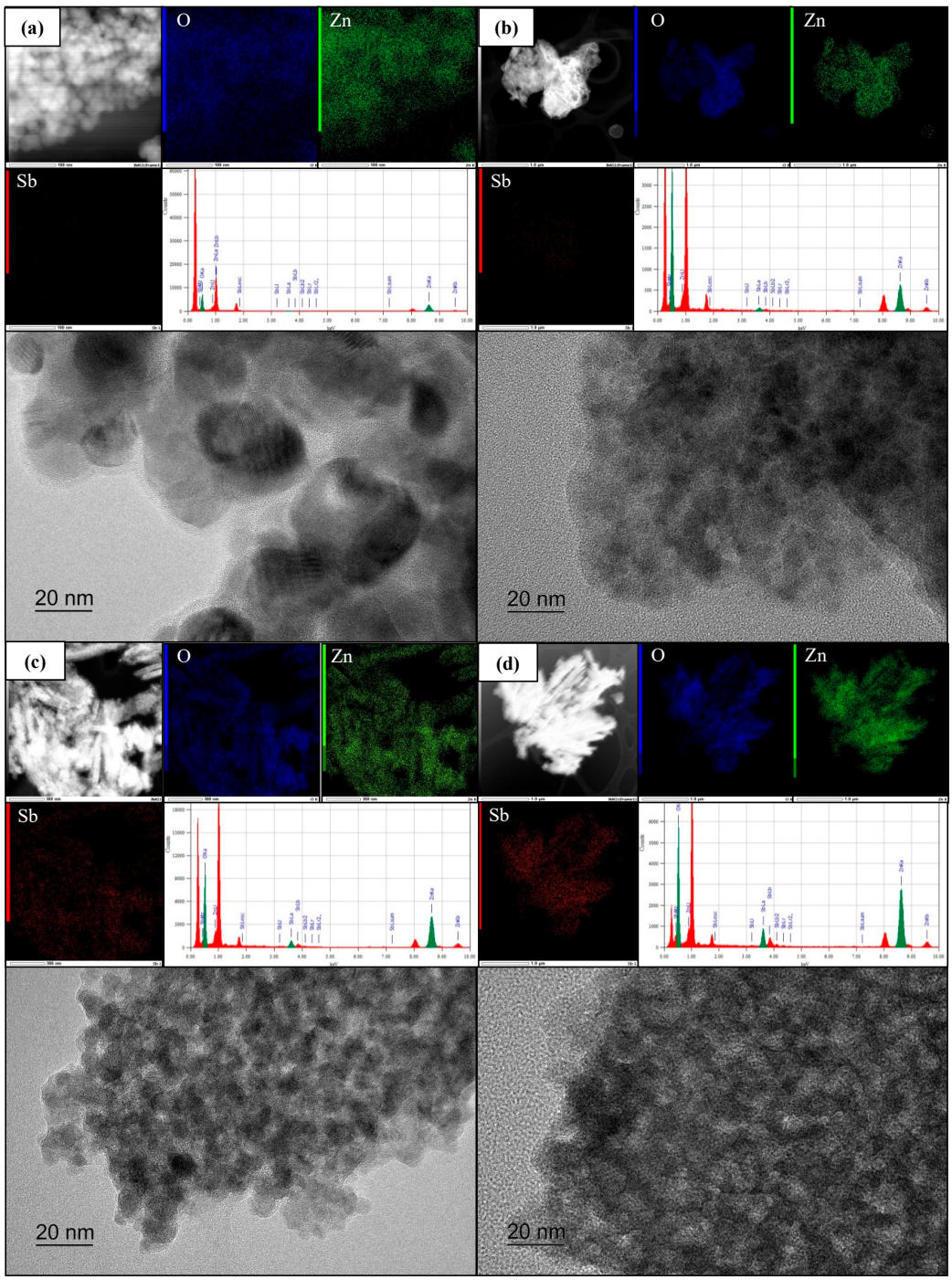

Figure 3. TEM images and EDS spectra of (a) undoped ZnO, (b) 3% Sb-doped ZnO, (c) 5% Sb-doped ZnO, (d) 10% Sb- doped ZnO.

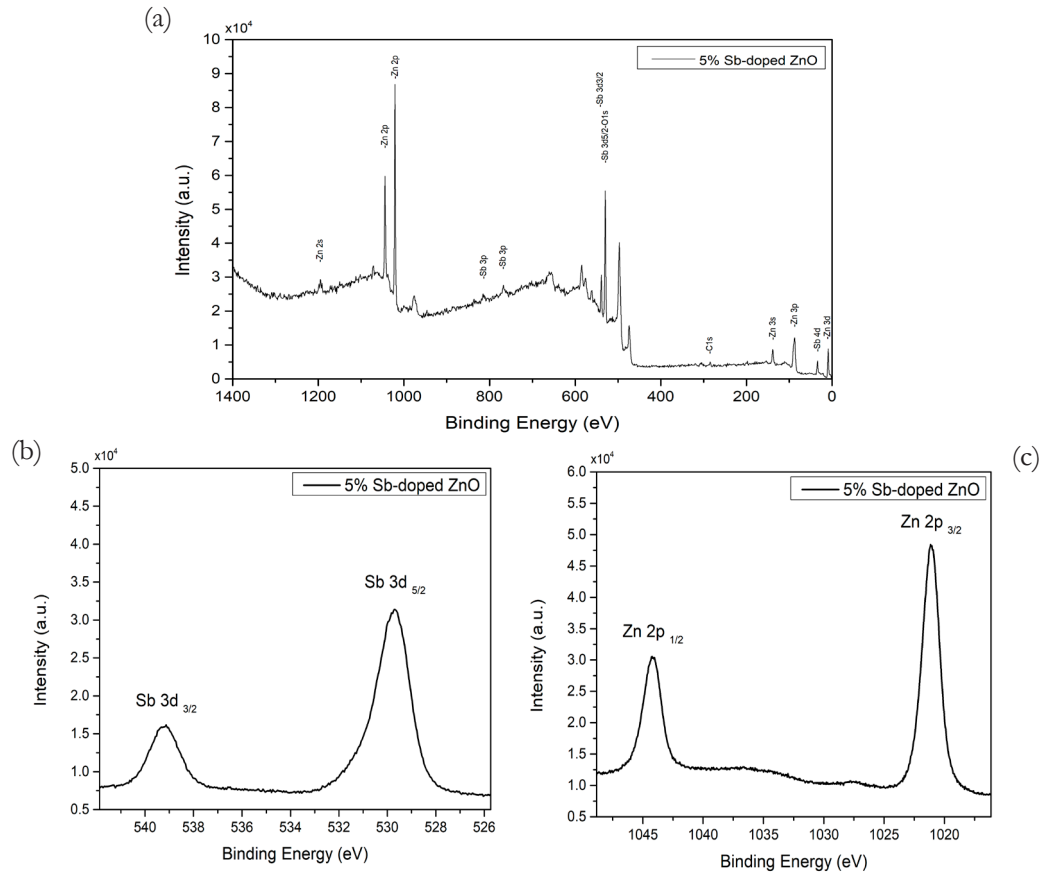

Figure 4. XPS spectra of 5% Sb-doped ZnO (a) survey scan, (b) Sb 3d spectra and (c) core-level Zn 2p spectra.

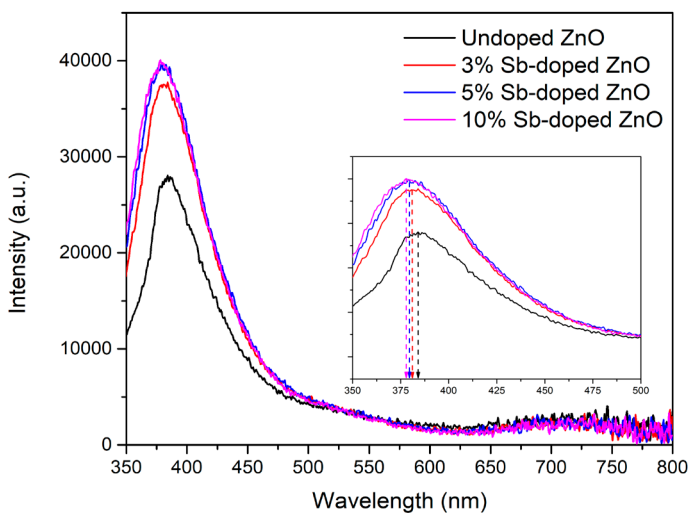

Figure 5. PL spectra of Sb-doped ZnO thin films with various doping concentrations.

Burstein-Moss effect and the other possible mechanism of quantum size effect [14, 11].

Figure 6 illustrates the transmittance spectra of Sb-doped ZnO thin films indicating high transparency in visible region of the prepared films. For the undoped and Sb-doped ZnO thin films, the corresponding transmittance spectra possess absorption edge around 375 nm with high transparency greater than 90%.

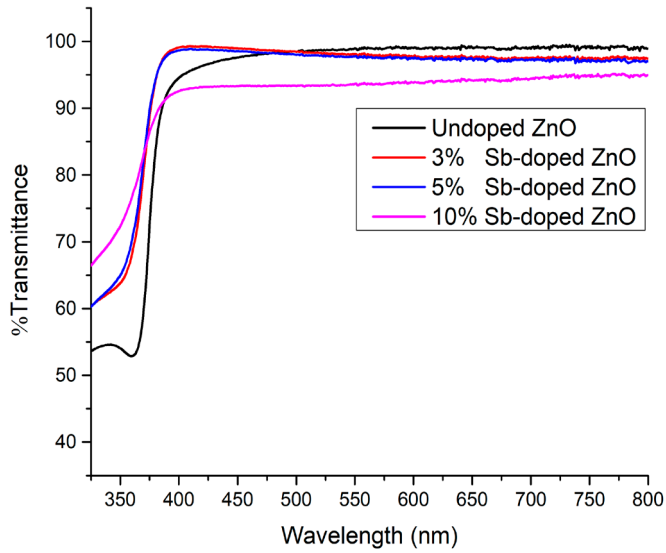

Figure 6. Transmittance spectra of Sb-doped ZnO thin films with various doping concentrations.

Table 1. EDS analysis of Sb-doped ZnO thin films.

Samples	Elements (atom %)		
	O	Zn	Sb
Undoped ZnO	73.86	26.14	n/a
3% Sb-doped ZnO	84.82	14.49	0.69
5% Sb-doped ZnO	69.80	27.30	2.90
10% Sb-doped ZnO	64.57	28.52	6.91

4. CONCLUSION

In conclusion, this work reports the preparation of Sb-doped ZnO thin films by sol-gel spin coating technique accompanying temperate annealing process. The XRD result shows that all prepared films possess ZnO hexagonal wurtzite structure without impurity phase. The XRD patterns indicate significant deterioration of ZnO phase since incorporated Sb atom could act as an inhibitor for ZnO grain growth that is in harmony with the FESEM and TEM images. TEM images revealed that the prepared films are composed of fine nanoparticles and their particle size decreases with increasing doping content. EDS spectra confirm the existence of Sb in the doped

samples with corresponding content. XPS spectra confirm Sb^{3+} incorporated in ZnO structure. PL results exhibit observable blue-shift in near band edge emission peak with noticeable deep-level defect emission. The transmittance spectra of all samples display high transparency in visible region.

Acknowledgements

This work has been supported by Thailand Research Fund (TRF) within the Royal Golden Jubilee Ph.D. Program (Grant no. PHD/0143/2559). The authors would like to thank Collage of Nanotechnology, King Mongkut's Institute of Technology Ladkrabang for supported the facility. Scientific instrument (TEM, PL) supported by the Frontier Research Center, Vidyasirimedhi Institute of Science and Technology, is gratefully acknowledged. For XPS experiments, authors would like to thank Synchrotron Light Research Institute (Public Organization) beamline 5.3 XPS (BL5.3: SUT−NANOTEC−SLRI).

References

[1] Hamrit S., Djessas K., Brihi N., Viallet B., Medjnoun K. and Grillo S.E., *Ceram. Int.*, 2016; **42**: 16212-16219. DOI 10.1016/j.ceramint.2016.07.143.

[2] Pradel K.C., Wu W., Zhou Y., Wen X., Ding Y. and Wang Z.L., *Nano Lett.*, 2013; **13**: 2647-2653. DOI: 10.1021/nl400792w.

[3] Akhtarianfar S.F., Khayatian A. and Almasi-Kashi M., *Ceram. Int.*, 2016; **42**: 13421-13431. DOI 10.1016/j.ceramint.2016.05.123.

[4] Galstyann V., Comini E., Baratto C., Faglia G. and Sberveglieri G., *Ceram. Int.*, 2015; **41**: 14239-14244. DOI 10.1016/j.ceramint.2015.07.052.

[5] Kwon Y.H., Kim D.H., Kim H.K. and Nah J., *Nano Energ.*, 2015; **18**: 126-132. DOI 10.1016/j.nanoen.2015.10.009.

[6] Bashar S.B., Suja M., Morshed M., Gao F. and Liu J., *Nanotechnology*, 2016; **27**: 065204. DOI 10.1088/0957-4484/27/6/065204.

[7] Kim J.B., Byun D., Ie S.Y., Park D.H., Choi W.K., Choi J.W. and Angadi B., *Semicond. Sci. Technol.*, 2008; **23:** 095004. DOI 10.1088/0268-1242/23/9/095004.

[8] Khosravi-Gandomani S., Yousefi R., Jamali-Sheini F. and Huang N.M., *Ceram. Int.*, 2014; **40**: 7957-7963. DOI 10.1016/j.ceramint.2013.12.145.

[9] Kim K., Debnath P.C., Lee D.H., Kim S. and Lee S.Y., *Nanoscale Res. Lett.*, 2001; **6**: 552. DOI 10.1186/1556-276X-6-552.

[10] Dang H.P., Luc Q.H., Le T. and Le V.H., *J. Nanomater.*, 2016; **2016**: Article ID 7825456 11 pp. DOI 10.1155/2016/7825456.

[11] Cheng Y., Yang K., Chen J., Che L. and Zhang X., *J. Alloy Compd.*, 2017; **699**: 690-694. DOI 10.1016/j.jallcom.2016.12.391.

[12] Noh W.S., Lee J.A., Lee J.H., Heo Y.W. and Kim J.J., *Ceram. Int.*, 2016; **42**: 4136-4142. DOI 10.1016/j.ceramint.2015.11.086.

[13] Noonuruk R., Vittayakorn N., Mekprasart W. and Pecharapa W., *J. Nanosci. Nanotechnol.*, 2015; **15**: 2564-2569. PMID: 26413706. PMID: 26413706.

[14] Bangbai C., Chongsri K., Pecharapa W., and Techidheera W., *Sains Malays.*, 2013; **42:** 239-246. DOI 10.1109/ESciNano.2012.6149675.

[15] Baek S.D., Biswas P., Kim J.W., Kim Y.C., Lee T.I. and Myoung J.M., *ACS Appl. Mater. Interf.*, 2016; **8**: 13018-13026. DOI 10.1021/acsami.6b03258.

[16] Senthil kumar E., Venkatesh S. and Ramachandra Rao M.S., *Appl. Phys. Lett.*, 2010; **96**: 232504. DOI 10.1063/1.3449122.